Modeling Cornelia de Lange Syndrome *in vitro* and *in vivo* reveals a role for cohesin complex in neuronal survival and differentiation

Daniele Bottai[1], Marco Spreafico[2], Anna Pistocchi[2], Grazia Fazio[3], Raffaella Adami[1], Paolo Grazioli[1], Adriana Canu[2], Cinzia Bragato[4,5], Silvia Rigamonti[1,3], Chiara Parodi[1], Gianni Cazzaniga[3], Andrea Biondi[6], Franco Cotelli[7], Angelo Selicorni[8] and Valentina Massa[1*]

1. Dipartimento di Scienze della Salute, Università degli Studi di Milano, Milan, 20142, Italy

2. Dipartimento di Biotecnologie Mediche e Medicina Traslazionale, Università degli Studi di Milano, Milan, 20090, Italy

3. Centro Ricerca Tettamanti, Clinica Pediatrica, Università degli Studi di Milano-Bicocca, Fondazione MBBM/Ospedale S. Gerardo, Monza, 20900, Italy

4. Fondazione IRCCS Istituto Neurologico C. Besta, Milano, 20131, Italy

5. PhD program in Neuroscience, University of Milano-Bicocca

6. Clinica Pediatrica, Università degli Studi di Milano-Bicocca, Fondazione MBBM/Ospedale S. Gerardo, Monza, 20900, Italy

7. Dipartimento di Bioscienze, Università degli Studi di Milano, Milan, 20131, Italy

8. UOC Pediatria, ASST Lariana, Como, 22042, Italy

The authors wish it to be known that, in their opinion, the first two authors should be regarded ad joint First Authors

[*] correspondence to: Valentina Massa

Dipartimento di Scienze della Salute

Downloaded from https://academic.oup.com/hmg/advance-article-abstract/doi/10.1093/hmg/ddy329/5098226 by Università degli Studi di Milano user on 28 October 2018

Università degli Studi di Milano

Via A. Di Rudinì, 8

20142 Milano

Italy

Valentina.Massa@unimi.it

Phone/Fax +390250323207

Downloaded from https://academic.oup.com/hmg/advance-article-abstract/doi/10.1093/hmg/ddy329/5098226 by Università degli Studi di Milano user on 28 October 2018

ABSTRACT

Cornelia de Lange Syndrome (CdLS), which is reported to affect about 1 in 10,000 to 30,000 newborns, is a multisystem organ developmental disorder with relatively mild to severe effects. Among others, intellectual disability represents an important feature of this condition.

Cornelia de Lange syndrome can result from mutations in at least five genes: *NIPBL (nipped-B-like protein)*, *SMC1A (structural maintenance of chromosomes 1A)*, *SMC3 (structural maintenance of chromosomes 3)*, *RAD21 (RAD21 Cohesin Complex Component)*, and *HDAC8 (Histone deacetylase 8)*. It is believed that mutations in these genes cause CdLS by impairing the function of the cohesin complex (to which all the aforementioned genes contribute to the structure or function), disrupting gene regulation during critical stages of early development.

Since intellectual disorder might result from alterations in neural development, in this work, we studied the role of *Hdac8* gene in mouse neural stem cells and in vertebrate (*D.rerio*) brain development by knock-down and chemical inhibition experiments. An underlying features of Hdac8 deficiency is an increased cell death in the developing neural tissues, either in mouse NSCs and in zebrafish embryos.

Downloaded from https://academic.oup.com/hmg/advance-article-abstract/doi/10.1093/hmg/ddy329/5098226 by Università degli Studi di Milano user on 28 October 2018

INTRODUCTION

During embryonic development and, in mouse, up to four weeks after birth, the brain is shaped by immature neurons generated in excessive number that die before maturation is completed. This process is fundamental for achieving optimal brain connectivity and a number of brain disorders have been associated with altered neuronal cell death (1, 2). It has also been shown that disturbing this finely-tuned developmental process exerts detrimental effects on cell composition and global brain activity impacting on cognition (3). Signals involved in this balance are numerous and vary both during developmental stages and within involved brain areas. Some signals are considered "core", thereby inhibiting cell death allowing for proliferation and differentiation, others are "neuron-type specific" reflecting differences in receptors expressed on the cell membrane (4, 5). Neurogenesis during embryonic development, hence, envisages excessive differentiated neurons that will be removed if not fully integrated, starting from a pool of progenitor cells named neural stem cells (NSCs). In lower mammals such as mice primitive (p)NSCs are present from embryonic day 5.5 (E5.5). At E7.5, neural induction begins and the forming neural tube gives rise to the brain and the spinal cord. The cell population composing the neural tube consists of a relatively homogenous population of neuroepithelial cells that proliferate and expand through symmetric division. In the developing embryo, radial glial cells comprise NSCs that divide symmetrically to increase pool size and originate progenitors that migrate away from the periventricular germinal zone (6). In adults, the subventricular zone (SVZ), which extends along the length of the lateral wall of the lateral ventricles, and the dentate gyrus of the hippocampus represent the two most important reservoirs of NSCs (7). NSCs self-renewal, expansion, division and differentiation are controlled by a number of factors, both extrinsic (such as morphogens) and intrinsic (such as epigenetic modifications). Among these, hierarchically prominent role has been shown for chromatin remodeling, including accessibility and histone modifications (8). Interestingly, Cornelia de Lange syndrome (CdLS) is a genetic disorder caused by mutations in genes codifying for proteins regulating both chromatin features (CdLS1 MIM 122470, CdLS2 MIM 300590, CdLS3 MIM

Downloaded from https://academic.oup.com/hmg/advance-article-abstract/doi/10.1093/hmg/ddy329/5098226 by Università degli Studi di Milano user on 28 October 2018

610759, CdLS4 MIM614701, CdLS5 MIM 300882). Indeed, 80% of CdLS patients present mutations in one of five genes: *NIPBL*, *SMC1A*, *SMC3*, *RAD21* and *HDAC8* (9). The first four genes are part of the cohesin complex, a multimeric structure controlling chromosomal cohesion in all eukaryotic cells (10). The fifth, *HDAC8* gene, encodes for a class I histone deacetylase, hence considered an "eraser" in the epigenetic machinery components (11) with a known target (SMC3) in the cohesin complex (12). The present study sought to ascertain HDAC8 role in mammalian NSCs capabilities and during vertebrate embryonic brain development, with a particular emphasis on cell death as previous studies have shown the fundamental role of cohesin complex to maintain viable cells during embryonic development in neural tissues, and given the importance of HDAC8 in regulating a master-regulator of cell death (i.e. p53) (13–18).

Downloaded from https://academic.oup.com/hmg/advance-article-abstract/doi/10.1093/hmg/ddy329/5098226 by Università degli Studi di Milano user on 28 October 2018

RESULTS

HDAC8 inhibition reduces murine NSCs proliferation rate, inducing apoptosis and differentiating capabilities

During the proliferative phase, cells continuously treated with a specific inhibitor of HDAC8 activity (PCI34051) showed a lower proliferative capability. The proliferation of PCI34051 treated - NSCs was significantly lower compared to controls, as shown in Fig. 1 A, in which the average of three experiments for each culture is shown. The slopes of the growth curves are significantly different ($p<0.044$) and the overall number of cells treated with PCI34051 decreased during culture whereas the number of the cells treated with DMSO (CTR) exponentially increased during the experiment. Analysis of cell death revealed a significant increase in apoptosis following treatment with the inhibitor (Fig. 1B).

Treatment with HDAC8 inhibitor caused a change in differentiation capabilities significantly reducing the levels of expression of β-Tubulin III $p<0.01$ (Fig. 2) of about 50% at both time points (Fig.2B and 2C).

Hdac8 *Silencing reduces murine NSCs proliferation rate and differentiating capabilities*

The knockdown of *Hdac8* transcript in NSCs using specific siRNAs induced a significant reduction of the proliferative capability. siRNAs effects were synergist, although of less impact compared to inhibitor treatment (Fig. 3). The knockdown of *Hdac8* transcript in NSCs induced a significant reduction of proliferation in all analyzed samples, with a stronger effect upon using a combination of HDAC8.1 and HDAB8.2 siRNA (10 nM each). Nevertheless, even the single treatments were able to induce a significant ($p< 0.05$; Sample A) or highly significant ($p<0.001$; Sample C) reduction of NSCs proliferation. The knockdown of *Hdac8* transcript in differentiating NSCs

Downloaded from https://academic.oup.com/hmg/advance-article-abstract/doi/10.1093/hmg/ddy329/5098226 by Università degli Studi di Milano user on 28 October 2018

reduces, about of 30%, in a not significant fashion the expression of β-Tubulin III (Fig.4), supporting the outcome observed following chemical inhibition.

Zebrafish hdac8 identification and expression analyses

The human HDAC8 amino-acid sequence was used as a query for identifying *in-silico* the zebrafish *hdac8* gene. NCBI (http://www.ncbi.nlm.nih.gov/BLAST/), ClustalW (http://www.ebi.ac.uk/Tools/clustalw/) and SMART (http://smart.embl-heidelberg.de/) tools were used for basic handling and analyses of the nucleotide and protein sequences. Zebrafish *hdac8* is present in a single copy on chromosome 7 (nucleotide position: 51,710,354-51,749,895).

Characterization of zebrafish *hdac8* expression, using RT-PCR techniques, revealed that the transcript was present from the first stages of development up to 4 days post fertilization (4 dpf), thus including maternal and zygotic transcription (Fig. 5A). Moreover, zebrafish *hdac8* was found to be expressed through development and in adult organs such as muscles, oocytes, brain and gut (Fig. 5B).

Whole-mount *in situ* hybridization (WISH) expression analyses in embryos at 24 hours post fertilization (24 hpf) with a specific probe for zebrafish *hdac8* showed the presence of the transcript in the central nervous system (CNS), specifically in the dorsal part and eyes (Fig. 5C-C''). Moreover, in line with the expression in adult organs, *hdac8* was expressed in muscles and gut (Fig. 5C). At 48 hpf *hdac8* was expressed in the CNS, eyes, muscles and fin buds (Fig. 5D-D'').

hdac8 *loss-of-function results in increased cell death in the central nervous system (CNS)*

Loss-of-function studies were carried out by injecting a morpholino (*hdac8*-MO; Gene Tools LLC, Philomath OR, USA), a modified antisense oligonucleotide which binds specifically to *hdac8* mRNA blocking the production of protein. Embryos were initially injected with different

Downloaded from https://academic.oup.com/hmg/advance-article-abstract/doi/10.1093/hmg/ddy329/5098226 by Università degli Studi di Milano user on 28 October 2018

concentrations of ATG- or splice-*hdac8*-MO (0.5, 1 and 1.5 pmol/embryo) in order to assess the dose-dependent effect. 1 pmole/embryo was identified as the dose capable of generating the greatest number of embryos with typical phenotypic defects without causing global or drastic alterations in the body-plane development. Embryos injected with 1 pmole/embryo of ATG- or splice-*hdac8*-MOs were developmentally abnormal with defects in the cephalic structures (eye size, structure of the CNS), and in the formation of the tail (curved tail). Similar morphological phenotypes were obtained with the injection of the two different morpholinos directed against *hdac8*. These defects were used as benchmark to classify *hdac8*-MO into two phenotypic classes (class I mild phenotype, and class II severe phenotype) (Fig. 6A-C'). The distribution of the phenotypical classes was comparable between the ATG- and splice-*hdac8*-MOs, strongly suggesting that the morphological defects were caused by *hdac8*-loss-of-function (Fig. 6D). To further validate the *hdac8*-MO efficiency, we analyzed Hdac8 protein levels in 24 hpf embryos injected with ATG- or splice-*hdac8*-MOs. Quantification analyses indicated that at this concentration, the efficiency of Hdac8 reduction was about 50% (Fig. 6E-F). Since splice-*hdac8*-MO was designed against the *hdac8* exon1-intron2 junction, the retention of intron1 in morphant embryos was verified by PCR technique (Fig. 6G).

CNS malformations are caused by augmented apoptosis rescued by WNT pathway activation

The abnormal development of cephalic CNS was associated with the presence of apoptotic/necrotic tissues. Hence, TUNEL assays were conducted in *hdac8*-loss-of-function embryos at 24 hpf for evaluating rate of programmed cell death. Analysis showed increased apoptosis at the level of the midbrain, hindbrain optic vesicles and spinal cord in embryos injected with *hdac8*-MO compared to the control embryos (Fig. 7A-B). As we have previously shown in zebrafish models of cohesinopathies (13, 14) that augmented apoptosis was caused by altered canonical WNT-pathway, *hdac8*-loss-of-function embryos were treated with lithium chloride (LiCl) for activating the WNT-pathway. Following treatment with LiCl, TUNEL assay showed significantly reduced levels of

Downloaded from https://academic.oup.com/hmg/advance-article-abstract/doi/10.1093/hmg/ddy329/5098226 by Università degli Studi di Milano user on 28 October 2018

apoptosis compared to control embryos (83.3% N= 42; Fig. 7C). Moreover, injecting an *in vitro* synthesized zebrafish *hdac8*-mRNA a rescue of the apoptotic phenotype caused by the splice-*hdac8*-MO was observed, confirming the role for *hdac8* in preventing apoptosis (Fig. 7D). For these experiments, the splice-*hdac8*-MO was utilized for avoiding the possible direct impact of the ATG-*hdac8*-MO against the injected *hdac8*-mRNA.

The efficacy and specificity of the *hdac8*-loss-of-function were extensively tested with the two *hdac8* morpholinos as shown in Fig. 8. Increased apoptosis was obtained with the injection of the ATG or splice-*hdac8*-MO (Fig. 8 B-C) in comparison to controls (A), the levels of apoptotic cells were increased in class II embryos with more severe phenotype than class I (Fig. 8 B'-C'). Moreover, to address a synergistic effect of the two morpholinos, we injected subcritical doses of ATG-*hdac8*-MO (0,5 pmol/embryo) or splice-*hdac8*-MO (0,5 pmol/embryo) that singularly did not cause any effects on cell death. When co-injected with subcritical doses of each MO, the typical apoptotic phenotype previously observed by means of full doses injections was found (Fig. 8D).

Downloaded from https://academic.oup.com/hmg/advance-article-abstract/doi/10.1093/hmg/ddy329/5098226 by Università degli Studi di Milano user on 28 October 2018

DISCUSSION

Regulation of neuronal cell death is a fundamental process during both embryonic and adult life (19). During embryonic development, neurons are produced in excess number probably to ensure an adequate number of nerve cells at birth (20). Increased apoptosis during brain development has been associated to abnormal morphology and to adult behavioral abnormalities (21). In the present study, inhibition of HDAC8 enzymatic activity leads to an excessive apoptosis both in murine NSCs and in the developing vertebrate brain. HDAC8 is a histone deacetylase known to act on SMC3 availability, hence it is considered a player in the cohesin complex (12). Indeed, deacetylation of SMC3 is a critical step for protein recycling in cells. Cohesins and condensins are protein complexes acting prominently as regulators of cell division, controlling DNA content separation in daughter cells. Intriguingly, germline mutations in both complexes are associated with human conditions affecting brain development. Biallelic mutations in condensin components *NCAPD2*, *NCAPH*, or *NCAPD3* cause microcephaly in humans (22). Dominant autosomal or X-linked mutations in cohesin complex genes cause CdLS, a congenital multiorgan syndrome that presents microcephaly and autistic self-aggressive behaviors (9). Previous studies on models of CdLS have reported increased cell death in the developing brain (13, 14, 23) associated to an impaired activation of the canonical WNT-pathway or mitotic imbalance in the rad21 model, in which molecular analyses have shown both by array and RNA-seq deregulation of the WNT pathway (24, 25). Canonical WNT-pathway is mediated by activation of β-catenin, reduced in CdLS models, that translocates in the cell nucleus where it binds to DNA for gene-expression regulation (26, 27). Among known targets, Cyclin D1 (CCND1) is extensively described (28). Notably, CCND1, is known to play a pivotal role during neurogenesis. Indeed, it has been shown that overexpression of the cdk4 (cyclin-dependent kinase 4)–cyclinD1 complex, positive regulators of cell-cycle progression, induces NSCs expansion (29). Moreover, several studies indicated that shortening of NSCs cell-cycle in embryonic and adult brain is sufficient for inhibiting neuronal differentiation (30, 31). Hence, we sought to evaluate a model of CdLS NSCs. We inhibited

Downloaded from https://academic.oup.com/hmg/advance-article-abstract/doi/10.1093/hmg/ddy329/5098226 by Università degli Studi di Milano user on 28 October 2018

196 HDAC8 using PCI34051, a chemical compound known to specifically act on HDAC8 deacetylase
197 activity (12) in proliferating and differentiating murine NSCs. Our results clearly showed that upon
198 HDAC8 inhibition NSCs reduce their capability of proliferating, confirming recent findings shown
199 in cell lines(32). Likely, this is due to the observed increased apoptosis and it does not translate into
200 an augmented differentiation as expected in physiological condition in smooth muscle (33) and
201 brain (34). It was already demonstrated, in cellular model of glioblastomas, that the knockdown of
202 another cohesin, SMC1A, led to the significant decrease in proliferation of U251 and U87MG cells
203 (35). These results are on line with our *in vitro* analysis of the role of HDAC8 in NSCs.
204 Importantly, we found a significant reduction in cells positive for the neuronal-marker β-Tubulin
205 III, indicating that their neurogenic differentiating capabilities are hampered. Importantly, it has
206 been recently shown that retinoic pathway response is impaired in CdLS patients fibroblasts,
207 suggesting a weaken activation following exposure to a master-player in neuronal differentiation
208 (36). A neuronal reduction in CdLS patients could explain part of the behavioral and morphological
209 features often reported after birth (as reviewed in (37, 38)). Hence, a detailed analysis in mammals
210 should be conducted for better dissecting this possibility. To note, the reported consistently high
211 expression of CdLS-cohesins in the developing mouse embryos and human adult central nervous
212 system, especially in hindbrain and hindbrain-derived structures (39), notwithstanding the non-
213 proliferative characteristics of such organs. In the present study, *D.rerio* models of *hdac8*-
214 deficiency, obtained by morpholino antisense injections confirmed an increased apoptosis in the
215 developing CNS associated with altered canonical WNT-pathway. Molecular and morphological
216 alterations could be rescued upon chemical activation by LiCl treatment as previously shown in
217 other CdLS models (13).

218 In conclusion, we report an association between HDAC8 inhibition –model of CdLS- and increased
219 cell death in the developing neural tissues, both *in vitro* and *in vivo* with a consequent reduction in
220 neuronal differentiation capabilities, which could be involved in the severe mental retardation
221 observed in Cornelia de Lange Syndrome.

Downloaded from https://academic.oup.com/hmg/advance-article-abstract/doi/10.1093/hmg/ddy329/5098226 by Università degli Studi di Milano user on 28 October 2018

MATERIALS AND METHODS

Neural Stem Cells

NSCs obtained from SVZ of 4 months old C57 BL6 male mice were used. Cells were cultivated in a medium containing epidermal growth factor (EGF) and fibroblast growth factor (FGF) (40–42). Three different cultures from three mice were used for the experiments.

PCI34051 treatment

Cells were firstly grown in a large culture flask and then plated in a 12 wells tissue culture plate at the concentration of 10,000 cell/cm^2. Experiments were performed in triplicate for each culture. For proliferating cells experiments, cultures were treated either with PCI34051 25 μM, a known HDAC8 inhibitor (12), and dimethyl sulfoxide (DMSO) 1:1000, a concentration that does not alter NSCs properties, such as proliferation and differentiation. After 5 days of culture, spheres were harvested and mechanically dissociated to single cells and counted. The fold change was determined dividing the total number of cells by the initial number of plated cells. Differentiation was achieved by plating cells in presence of adhesion molecules Cultrex (Tema Ricerca, Italy) and in absence of growth factors. In a 48 wells plate, round sterile coverslip of the diameter of 1 cm was inserted. Wells were coated with 150 μl of Cultrex for one hour and 40,000 cells were loaded with 500 μl of medium containing FGF but not EGF (40–42) for two days. Following growth factor removal, treatment with HDAC8 inhibitor was started. Two different time points (from day 3 to day 7 and from day 5 to day 7) were used. As control, treated cells with DMSO 1:1000 for days 3 to 7 were used. At the end of the treatment, the medium was removed, the cells washed once with PBS and fixed with 4% paraformaldehyde for 10 min. Cells were then washed once with PBS and either used for immunocytochemistry or stored at 4 C°. Experiments were run in duplicates.

Downloaded from https://academic.oup.com/hmg/advance-article-abstract/doi/10.1093/hmg/ddy329/5098226 by Università degli Studi di Milano user on 28 October 2018

246 ***Silencing NSCs***

247 A 48 multiwell plate was coated with laminin (Synthetic Laminin Peptide, Sigma SCR127) using a
248 concentration of 150 ug/ml as suggested by the supplier. Two siRNAs (Qiagen) expected to anneal
249 different regions of the HDAC8 transcript (Flexitube siRNA 5 nmol cat nr SI01063895 and cat nr
250 SI01063902) were used. As negative control AllStars Negative Control siRNA (cat nr 1027280)
251 with no homology to any known mammalian genes and minimal nonspecific effects was selected.
252 HiPerFect Transfection Reagent (Qiagen) was used for siRNAs delivery. Four different cultures of
253 NSCs were used, and experiments were run in triplicates. We first plated dissociated cells (10,000
254 cells per well) on laminin-coated wells as a monolayer in 500 µl of proliferative medium (PM) for
255 one day. The following day, incubation medium (with siRNAs and Transfection Reagent prepared
256 following the manufacturer instruction) was added drop-wise onto the attached cells that were
257 incubated under their normal growth conditions for 3 hours before adding the PM medium. The
258 medium was changed after 24 hours and cells were cultured for 2-3 days. The cells were then
259 harvested, dissociated and counted. siRNAs concentrations were selected in pilot studies, choosing
260 20 nM as experimental concentration. For analyses of *Hdac8* silencing in differentiating NSCs, 3
261 different cultures were used.

262

263 ***Immunostaining of differentiated NSC***

264 Differentiation capabilities were assayed by means of immunostaining. For this purpose, antibodies
265 against glial fibrillary acidic protein, (GFAP, 1:250, Immunological Sciences AB-10635), and β-
266 Tubulin III (1:250, Immunological Sciences AB-10288) were used. Briefly, fixed cells were
267 permeabilized with 0.1 % Triton-X in PBS for 10 min at room temperature, then the primary
268 antibodies were added overnight at 4 °C in PBS with 10% normal goat serum (NGS). Secondary
269 antibodies conjugated with fluorophores were used: Alexa-fluor 488 (Goat anti mouse
270 Immunological Sciences IS20010) and Alexa-fluor 555 (Goat anti rabbit Immunological Sciences

Downloaded from https://academic.oup.com/hmg/advance-article-abstract/doi/10.1093/hmg/ddy329/5098226 by Università degli Studi di Milano user on 28 October 2018

IS20012). Nuclei were stained with 4′,6-Diamidine-2′-phenylindole dihydrochloride (DAPI) 300 nM (43). Images were acquired using a Leica SP2 microscope with He/Ne and Ar/Kr lasers. The number of positive cells was counted and compared within treatments. Experiments were repeated twice. A minimum of 1400 cells for each sample and for each treatment were counted.

Apoptosis assay

Apoptosis in NSCs was quantified using a Caspase-3/CPP32 Colorimetric Assay (BioVision) following manufacturer's protocol. Briefly, NSCs were harvested after 5 days of culture, resuspended in chilled lysis buffer, centrifuged and supernatant (representing cytosolic extract) was used. Following protein concentration measurement, spectrophotometric detection of the chromophore p-nitroaniline (pNA) after cleavage from the labeled substrate DEVD-pNA allowed for cell death assessment. Samples were run as experimental triplicates and technical duplicates.

Animals

Breeding wild type fish (zebrafish, *Danio rerio)* of the AB strain were maintained at 28°C on a 14 h light/10 h dark cycle. Embryos were collected by natural spawning, staged according to Kimmel and colleagues (44) and raised at 28°C in fish water (Instant Ocean, 0,1% Methylene Blue) in Petri dishes, according to established techniques. Zebrafish embryos were raised and maintained under standard conditions and national guidelines (Italian decree 4th March 2014, n.26). All experimental procedures were approved by IACUC (Institutional Animal Care and Use Committee, N. OPBA_93_2017). Embryonic ages are expressed in hours post fertilization (hpf) and days post fertilization (dpf).

Downloaded from https://academic.oup.com/hmg/advance-article-abstract/doi/10.1093/hmg/ddy329/5098226 by Università degli Studi di Milano user on 28 October 2018

Lithium chloride (LiCl) was added to fish water for 30 min at the 10-12 somite stage at a concentration of 0.3 M at 28°C as previously described (13). Treated embryos were then washed three times with water and allowed to develop to 24 hpf.

Reverse transcription-PCR assays (RT-PCR)

Total RNA from 12 samples (an average of 30 embryos per sample) was extracted with the TOTALLY RNA isolation kit (Ambion, Life Technologies, Paisley UK), treated with RQ1 RNase-Free DNase (Promega Madison WI, USA) and oligo(dT)-reverse transcribed using SuperScript II RT (Invitrogen, Carlsbad, CA, USA), according to manufacturers' instructions. PCR products were loaded and resolved onto 1% agarose gels. The β-actin expression was tested in parallel with the gene of interest as a housekeeping gene control for the cDNA loaded.

Following primers were used:

*hdac8pr*_sense 5'-ACATGAGGGTCGTGAAGCCT-3'
*hdac8pr*_antisense 5'-ACCGCGTCATTCACATAACA-3'
*hdac8fl*_sense 5'-ATGAGTGAAAAAAGCGACAG-3',
*hdac8fl*_antisense 5'- CGATCCTAAACTACATTCTTC-3'.
*hdac8E1*_sense 5'-GTCCAAAGTCAGCAGACT-3',
*hdac8I2*_antisense 5'-GTGAGATGAACTGCACTCT-3'

In situ *hybridization and histological analysis*

Whole Mount *In Situ* hybridization (WISH) experiments were carried out as described by Thisse and colleagues (45). For each experiment a minimum of 30 controls and MO-injected embryos were analyzed. *hdac8* probe was cloned using RT-PCR primers. For histological sections, stained embryos were re-fixed in 4% PFA, dehydrated and stored in methanol, wax embedded and

Downloaded from https://academic.oup.com/hmg/advance-article-abstract/doi/10.1093/hmg/ddy329/5098226 by Università degli Studi di Milano user on 28 October 2018

sectioned (5 μm). Images of embryos and sections were acquired using a microscope equipped with digital camera with LAS Leica Imaging software (Leica, Wetzlar, Germany). Images were processed using Adobe Photoshop software and, when necessary, different focal planes of the same image have been taken separately and later merged in a single image.

TUNEL staining

For TUNEL assay, a minimum of 24 embryos (per experimental group) were fixed in 4% PFA for 2 h at room temperature. Embryos were washed with methanol at –20°C and then twice with PBC (0.001% Triton X-100, 0.1% sodium citrate in PBS) for 10 minutes. Staining for apoptotic cells was performed using the AP-*In situ* Cell Death Detection Kit (Roche Diagnostics, Penzberg, Germany) carefully leaving labeling reagents to react for the same length of time for all experiments. Embryos were incubated at 37°C for 1 h and fluorescent apoptotic cells were detected under a fluorescent microscope (Leica). For the visual staining, embryos were then washed, stained and mounted for microscopic imaging.

Injections

To repress *hdac8* mRNA translations, two morpholinos were synthesized (Gene Tools LLC, Philomath OR, USA) targeting *hdac8*-ATG and exon1-intron1 junction (splice-*hdac8*-MO) (46).

ATG-*hdac8*-MO: 5'-CATTACTGTCGCTTTTTTCACTCAT-3',

splice-*hdac8*-MO: 5'-TGCAGAGTGCAGTTCATCTCACCCG-3',

and used at the concentration of 1 pmole/embryo in 1x Danieau buffer (pH 7,6). A standard control morpholino oligonucleotide (ctrl-MO) was injected in parallel (47). When co-injected, ATG- and splice-*hdac8*-MOs were used at subcritical doses of 0,5 pmole/embryo in 1x Danieau buffer (pH

Downloaded from https://academic.oup.com/hmg/advance-article-abstract/doi/10.1093/hmg/ddy329/5098226 by Università degli Studi di Milano user on 28 October 2018

7,6). In all experiments, *hdac8*-MO-injected embryos were compared to embryos injected with the same amount of ctrl-MO at the same developmental stage. For the *in vivo* test of the specificity of morpholino-mediated knockdown, the rescue of morphants phenotype was evaluated by co-injecting zebrafish *hdac8*-mRNA at the concentration of 500 pg/embryo.

Western blot

Fish embryos (minimum 30 per experimental group) were lysated in RIPA buffer (5 µl for each embryo), and homogenized. Samples were boiled for 10 min at 95°C. 20 µl of protein sample was size-fractionated by gel Pre-cast (Invitrogen) and transferred with iBlot (Invitrogen). The nitrocellulose membranes were blocked with 5% nonfat dry milk in PBST (PBS containing 0.1% Tween 20) for 30 min at room temperature and subsequently incubated with the primary antibody: rabbit anti-Hdac8 (1:1000, HDAC8 (H-145) sc-11405, Santa Cruz Biotechnology, Santa Cruz, CA, USA) and mouse anti-GAPDH (1:2500, DSHB)) and mouse anti-Vinculin (1:6000, Sigma), diluted in 4% milk/PBST over night at 4°C. Horseradish peroxidase-conjugated secondary antibody (Sigma Aldrich, St Louis MO, USA) was used for 1 hour at room temperature. The antigen signal was detected with the ECL chemiluminescence detection system (Amersham, Piscataway, NJ, USA) as specified by the manufacturer.

Data Analysis

Proliferation statistical analysis was performed using student's t-test. NSCs immunostaining analysis was performed using the One-way analysis of variance followed by Bonferroni's Multiple Comparison Test. Apotosis assay was analysed using student's t-test. $p \leq 0.05$ was set as statistically significant. For graphs Graphpad Prism software and for figures Adobe Photoshop were used.

Downloaded from https://academic.oup.com/hmg/advance-article-abstract/doi/10.1093/hmg/ddy329/5098226 by Università degli Studi di Milano user on 28 October 2018

ACKNOWLEDGMENTS

The authors are grateful to the Italian National Association of Volunteers Cornelia de Lange for support and inspiration. The authors want to express their deepest gratitude to Dr Julia Horsfield for manuscript commenting. This work was supported by Fondazione Cariplo, grant n. 2015-0783 to VM, by Università degli Studi di Milano-Dipartimento DISS-Linea B to VM, Universita' degli Studi di Milano-Dipartimento BIOMETRA-Linea B to AP and by Fondazione Mariani (Como, Italy) to AS, and to PhD program in Molecular and Translational Science-Università degli Studi di Milano scholarship to PG.

CONFLICT OF INTEREST

The authors declare no conflict of interest.

Downloaded from https://academic.oup.com/hmg/advance-article-abstract/doi/10.1093/hmg/ddy329/5098226 by Università degli Studi di Milano user on 28 October 2018

REFERENCES

1. Ribe,E.M., Serrano-Saiz,E., Akpan,N. and Troy,C.M. (2008) Mechanisms of neuronal death in disease: defining the models and the players. *Biochem. J.*, **415**, 165–182.

2. Martin,L.J. (2001) Neuronal cell death in nervous system development, disease, and injury (Review). *Int. J. Mol. Med.*, **7**, 455–478.

3. Pfisterer,U. and Khodosevich,K. (2017) Neuronal survival in the brain: neuron type-specific mechanisms. *Cell Death Dis.*, **8**, e2643.

4. Temple,S. (2001) The development of neural stem cells. *Nature*, **414**, 112–117.

5. Gage,F.H. (2000) Mammalian Neural Stem Cells. *Science (80-.).*, **287**, 1433–1438.

6. Xu,W., Lakshman,N. and Morshead,C.M. (2017) Building a central nervous system: The neural stem cell lineage revealed. *Neurogenesis*, **4**, e1300037.

7. Daniela,F., Vescovi,A.L. and Bottai,D. (2007) The stem cells as a potential treatment for neurodegeneration. *Methods Mol. Biol.*, **399**, 199–213.

8. Gaspar-Maia,A., Alajem,A., Meshorer,E. and Ramalho-Santos,M. (2011) Open chromatin in pluripotency and reprogramming. *Nat. Rev. Mol. Cell Biol.*, **12**, 36–47.

9. Deardorff,M.A., Noon,S.E. and Krantz,I.D. (1993) Cornelia de Lange Syndrome.

10. Hagstrom,K.A. and Meyer,B.J. (2003) Condensin and cohesin: more than chromosome compactor and glue. *Nat. Rev. Genet.*, **4**, 520–534.

11. Bjornsson,H.T. (2015) The Mendelian disorders of the epigenetic machinery. *Genome Res.*, **25**, 1473–1481.

12. Deardorff,M.A., Bando,M., Nakato,R., Watrin,E., Itoh,T., Minamino,M., Saitoh,K., Komata,M.,

Downloaded from https://academic.oup.com/hmg/advance-article-abstract/doi/10.1093/hmg/ddy329/5098226 by Università degli Studi di Milano user on 28 October 2018

Katou,Y., Clark,D., *et al.* (2012) HDAC8 mutations in Cornelia de Lange syndrome affect the cohesin acetylation cycle. *Nature*, **489**, 313–317.

13. Pistocchi,A., Fazio,G., Cereda,A., Ferrari,L., Bettini,L.R., Messina,G., Cotelli,F., Biondi,A., Selicorni,A. and Massa,V. (2013) Cornelia de Lange Syndrome: NIPBL haploinsufficiency downregulates canonical Wnt pathway in zebrafish embryos and patients fibroblasts. *Cell Death Dis.*, **4**, e866.

14. Fazio,G., Gaston-Massuet,C., Bettini,L.R., Graziola,F., Scagliotti,V., Cereda,A., Ferrari,L., Mazzola,M., Cazzaniga,G., Giordano,A., *et al.* (2016) CyclinD1 Down-Regulation and Increased Apoptosis Are Common Features of Cohesinopathies. *J. Cell. Physiol.*, **231**, 613–622.

15. Yan,W., Liu,S., Xu,E., Zhang,J., Zhang,Y., Chen,X. and Chen,X. (2013) Histone deacetylase inhibitors suppress mutant p53 transcription via histone deacetylase 8. *Oncogene*, 10.1038/onc.2012.81.

16. Qi,J., Singh,S., Hua,W.K., Cai,Q., Chao,S.W., Li,L., Liu,H., Ho,Y., McDonald,T., Lin,A., *et al.* (2015) HDAC8 Inhibition Specifically Targets Inv(16) Acute Myeloid Leukemic Stem Cells by Restoring p53 Acetylation. *Cell Stem Cell*, 10.1016/j.stem.2015.08.004.

17. Wu,J., Du,C., Lv,Z., Ding,C., Cheng,J., Xie,H., Zhou,L. and Zheng,S. (2013) The up-regulation of histone deacetylase 8 promotes proliferation and inhibits apoptosis in hepatocellular carcinoma. *Dig. Dis. Sci.*, 10.1007/s10620-013-2867-7.

18. Hua,W.K., Qi,J., Cai,Q., Carnahan,E., Ramirez,M.A., Li,L., Marcucci,G. and Kuo,Y.H. (2017) HDAC8 regulates long-term hematopoietic stem-cell maintenance under stress by modulating p53 activity. *Blood*, 10.1182/blood-2017-03-771386.

19. Hutchins,J.B. and Barger,S.W. (1998) Why neurons die: Cell death in the nervous system. *Anat.*

Downloaded from https://academic.oup.com/hmg/advance-article-abstract/doi/10.1093/hmg/ddy329/5098226 by Università degli Studi di Milano user on 28 October 2018

Rec., **253**, 79–90.

20. Dekkers,M.P.J., Nikoletopoulou,V. and Barde,Y.A. (2013) Death of developing neurons: New insights and implications for connectivity. *J. Cell Biol.*, **203**, 385–393.

21. Broad,K.D., Curley,J.P. and Keverne,E.B. (2009) Increased apoptosis during neonatal brain development underlies the adult behavioral deficits seen in mice lacking a functional paternally expressed gene 3 (Peg3). *Dev. Neurobiol.*, **69**, 314–325.

22. Martin,C.A., Murray,J.E., Carroll,P., Leitch,A., Mackenzie,K.J., Halachev,M., Fetit,A.E., Keith,C., Bicknell,L.S., Fluteau,A., *et al.* (2016) Mutations in genes encoding condensin complex proteins cause microcephaly through decatenation failure at mitosis. *Genes Dev.*, **30**, 2158–2172.

23. Horsfield,J.A., Anagnostou,S.H., Hu,J.K.-H., Cho,K.H.Y., Geisler,R., Lieschke,G., Crosier,K.E. and Crosier,P.S. (2007) Cohesin-dependent regulation of Runx genes. *Development*, **134**, 2639–2649.

24. Rhodes,J.M., Bentley,F.K., Print,C.G., Dorsett,D., Misulovin,Z., Dickinson,E.J., Crosier,K.E., Crosier,P.S. and Horsfield,J.A. (2010) Positive regulation of c-Myc by cohesin is direct, and evolutionarily conserved. *Dev. Biol.*, 10.1016/j.ydbio.2010.05.493.

25. Schuster,K., Leeke,B., Meier,M., Wang,Y., Newman,T., Burgess,S. and Horsfield,J.A. (2015) A neural crest origin for cohesinopathy heart defects. *Hum. Mol. Genet.*, 10.1093/hmg/ddv402.

26. Tortelote,G.G., Reis,R.R., de Almeida Mendes,F. and Abreu,J.G. (2017) Complexity of the Wnt/β-catenin pathway: Searching for an activation model. *Cell. Signal.*, **40**, 30–43.

27. Clevers,H., Barker,N. and Morin,P.J. (2000) The Yin-Yang of TCF/beta-catenin signaling. *Adv. Cancer Res.*, **77**, 1–24.

28. Shtutman,M., Zhurinsky,J., Simcha,I., Albanese,C., D'Amico,M., Pestell,R. and Ben-Ze'ev, a

Downloaded from https://academic.oup.com/hmg/advance-article-abstract/doi/10.1093/hmg/ddy329/5098226 by Università degli Studi di Milano user on 28 October 2018

(1999) The cyclin D1 gene is a target of the beta-catenin/LEF-1 pathway. *Proc. Natl. Acad. Sci. U. S. A.*, **96**, 5522–5527.

29. Lange,C., Huttner,W.B. and Calegari,F. (2009) Cdk4/CyclinD1 Overexpression in Neural Stem Cells Shortens G1, Delays Neurogenesis, and Promotes the Generation and Expansion of Basal Progenitors. *Cell Stem Cell*, **5**, 320–331.

30. Salomoni,P. and Calegari,F. (2010) Cell cycle control of mammalian neural stem cells: Putting a speed limit on G1. *Trends Cell Biol.*, **20**, 233–243.

31. Artegiani,B., Lange,C. and Calegari,F. (2012) Expansion of embryonic and adult neural stem cells by in utero electroporation or viral stereotaxic injection. *J. Vis. Exp.*, 10.3791/4093.

32. Dasgupta,T., Antony,J., Braithwaite,A.W. and Horsfield,J.A. (2016) HDAC8 Inhibition Blocks SMC3 Deacetylation and Delays Cell Cycle Progression without Affecting Cohesin-dependent Transcription in MCF7 Cancer Cells. *J. Biol. Chem.*, 10.1074/jbc.M115.704627.

33. Waltregny,D., De Leval,L., Glénisson,W., Ly Tran,S., North,B.J., Bellahcène,A., Weidle,U., Verdin,E. and Castronovo,V. (2004) Expression of histone deacetylase 8, a class I histone deacetylase, is restricted to cells showing smooth muscle differentiation in normal human tissues. *Am. J. Pathol.*, **165**, 553–564.

34. Murko,C., Lagger,S., Steiner,M., Seiser,C., Schoefer,C. and Pusch,O. (2010) Expression of class i histone deacetylases during chick and mouse development. *Int. J. Dev. Biol.*, **54**, 1525–1535.

35. Yang,Y., Zhang,Z., Wang,R., Ma,W., Wei,J. and Li,G. (2013) SiRNA-mediated knockdown of SMC1A expression suppresses the proliferation of glioblastoma cells. *Mol. Cell. Biochem.*, 10.1007/s11010-013-1704-9.

36. Fazio,G., Bettini,L.R., Rigamonti,S., Meta,D., Biondi,A., Cazzaniga,G., Selicorni,A. and

Downloaded from https://academic.oup.com/hmg/advance-article-abstract/doi/10.1093/hmg/ddy329/5098226 by Università degli Studi di Milano user on 28 October 2018

Massa,V. (2017) Impairment of Retinoic Acid Signaling in Cornelia de Lange Syndrome Fibroblasts. *Birth Defects Res.*, **109**, 1268–1276.

37. Avagliano,L., Grazioli,P., Mariani,M., Bulfamante,G.P., Selicorni,A. and Massa,V. (2017) Integrating molecular and structural findings: Wnt as a possible actor in shaping cognitive impairment in Cornelia de Lange syndrome. *Orphanet J. Rare Dis.*, **12**.

38. Avagliano,L., Bulfamante,G. Pietro and Massa,V. (2017) Cornelia de lange syndrome: To diagnose or not to diagnose in utero? *Birth Defects Res.*, **109**, 771–777.

39. Bettini,L.R., Graziola,F., Fazio,G., Grazioli,P., Scagliotti,V., Pasquini,M., Cazzaniga,G., Biondi,A., Larizza,L., Selicorni,A., *et al.* (2018) Rings and bricks: Expression of cohesin components is dynamic during development and adult life. *Int. J. Mol. Sci.*, **19**.

40. Gelain,F., Bottai,D., Vescovi,A. and Zhang,S. (2006) Designer self-assembling peptide nanofiber scaffolds for adult mouse neural stem cell 3-dimensional cultures. *PLoS One*, **1**, e119.

41. Henry,G.R.P., Heise,A., Bottai,D., Formenti,A., Gorio,A., Di Giulio,A.M. and Koning,C.E. (2008) Acrylate end-capped poly(ester-carbonate) and poly(ether-ester)s for polymer-on-multielectrode array devices: Synthesis, photocuring, and biocompatibility. *Biomacromolecules*, **9**, 867–878.

42. Adami,R., Pagano,J., Colombo,M., Platonova,N., Recchia,D., Chiaramonte,R., Bottinelli,R., Canepari,M. and Bottai,D. (2018) Reduction of movement in neurological diseases: Effects on neural stem cells characteristics. *Front. Neurosci.*, 10.3389/fnins.2018.00336.

43. Bottai,D., Scesa,G., Cigognini,D., Adami,R., Nicora,E., Abrignani,S., Di Giulio,A.M. and Gorio,A. (2014) Third trimester NG2-positive amniotic fluid cells are effective in improving repair in spinal cord injury. *Exp. Neurol.*, 10.1016/j.expneurol.2014.01.015.

Downloaded from https://academic.oup.com/hmg/advance-article-abstract/doi/10.1093/hmg/ddy329/5098226 by Università degli Studi di Milano user on 28 October 2018

489 44. Kimmel,C.B., Ballard,W.W., Kimmel,S.R., Ullmann,B. and Schilling,T.F. (1995) Stages of
490 embryonic development of the zebrafish. *Dev. Dyn.*, **203**, 253–310.

491 45. Thisse,C., Thisse,B., Schilling,T.F. and Postlethwait,J.H. (1993) Structure of the zebrafish
492 snail1 gene and its expression in wild-type, spadetail and no tail mutant embryos.
493 *Development*, **119**, 1203–1215.

494 46. Ferrari,L., Bragato,C., Brioschi,L., Spreafico,M., Esposito,S., Pezzotta,A., Pizzetti,F., Moreno-
495 Fortuny,A., Bellipanni,G., Giordano,A., *et al.* (2018) HDAC8 regulates canonical Wnt
496 pathway to promote differentiation in skeletal muscles. *J. Cell. Physiol.*, **1**.

497 47. Nasevicius, a and Ekker,S.C. (2000) Effective targeted gene 'knockdown' in zebrafish. *Nat.*
498 *Genet.*, **26**, 216–20.

499

500

Downloaded from https://academic.oup.com/hmg/advance-article-abstract/doi/10.1093/hmg/ddy329/5098226 by Università degli Studi di Milano user on 28 October 2018

FIGURE LEGENDS

Figure 1. Growth curve and apoptosis of the PCI34051 treated cells

Reddish colors represent the controls, greenish colors represent PCI34051 treated cells. A) in red #A DMSO; in purple #B DMSO, in pink #C DMSO, in light green #A PCI34051; in green #B PCI34051, in bright green #C PCI34051, in purple with dashed line represents the mean of the three samples treated with DMSO; in green with dashed line represents the mean of the samples treated with PCI34051. B) apoptosis levels induced by PCI34051 treatment expressed as absorbance (Y axis) per samples (X axis).

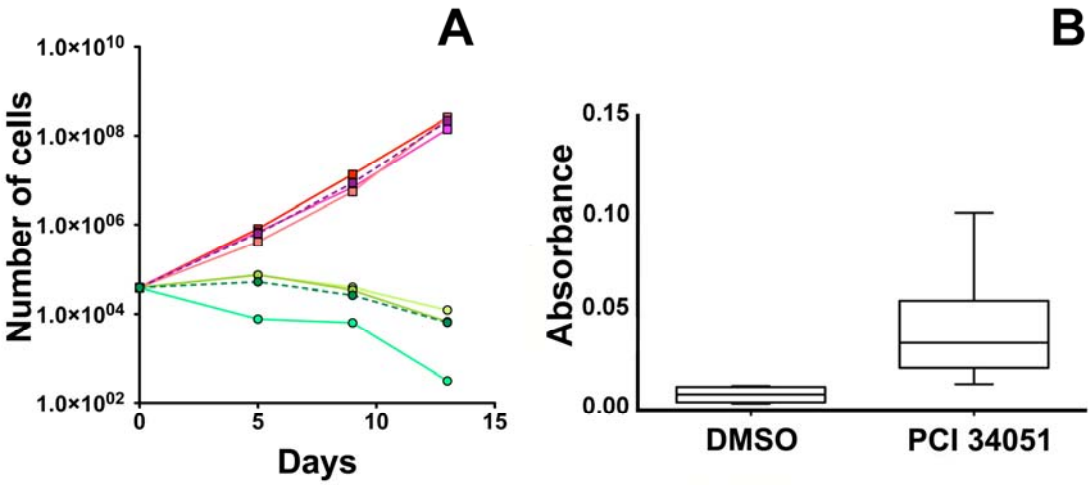

Downloaded from https://academic.oup.com/hmg/advance-article-abstract/doi/10.1093/hmg/ddy329/5098226 by Università degli Studi di Milano user on 28 October 2018

Figure 2. Immunofluorescence analysis of NSCs differentiation

A) DMSO treated sample (controls) B) PCI34051 treated sample for 3 days; C) PCI34051 treated sample for 5 days, A') magnification of white box in A showing β-Tubulin III and GFAP positive cells. D) White column CTR (DMSO treated), grey column PCI34051 treated cell between days 5-7 of the differentiation, black column PCI34051 treated cell between days 3-7 of the differentiation. **=p<0.0017. Scale bar indicates in A=25μm, in A' =10 μm; Blue DAPI, green GFAP, red β-Tubulin III.

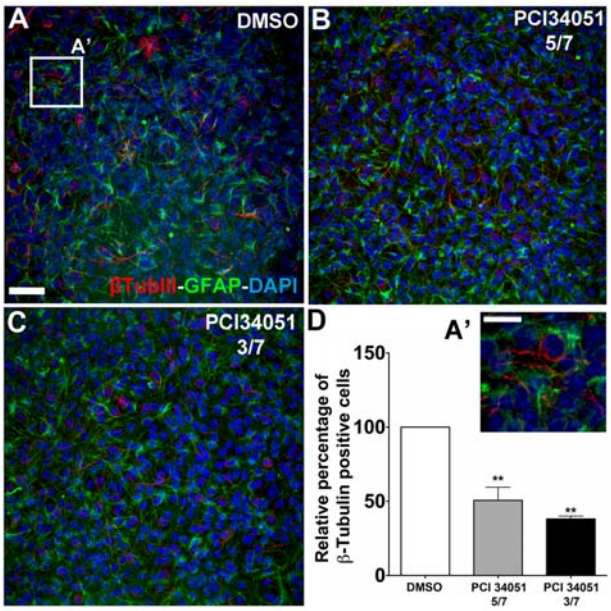

Downloaded from https://academic.oup.com/hmg/advance-article-abstract/doi/10.1093/hmg/ddy329/5098226 by Università degli Studi di Milano user on 28 October 2018

Figure 3. Proliferative changes induced in NSCs by the knockdown of *Hdac8* NSCs

The knockdown of *Hdac8* transcript causes a significant reduction of NSCs proliferation in all three analyzed cultures. The analysis was performed comparing also PCI34051 effects. Bars represent from left to right , for each dataset, CTR, PCI34051, CTR siRNA, HDAC8.1, HDAC8.2, HDAC8.1+HDAC8.2.

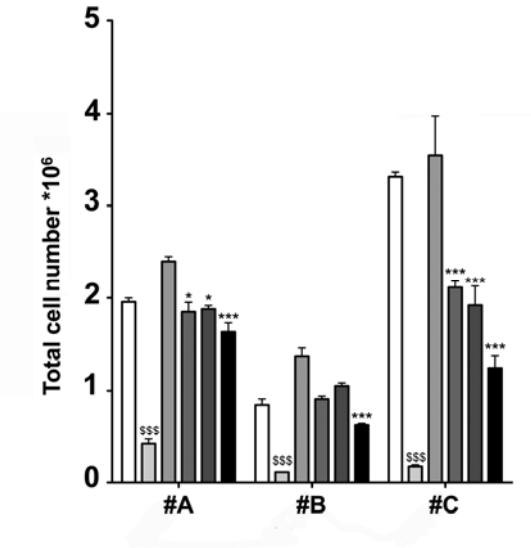

Downloaded from https://academic.oup.com/hmg/advance-article-abstract/doi/10.1093/hmg/ddy329/5098226 by Università degli Studi di Milano user on 28 October 2018

Figure 4. Changes in differentiation induced in NSCs by the knockdown of *Hdac8* NSCs

The knockdown of *Hdac8* transcript causes an alteration of NSCs differentiation. The analysis was performed comparing also PCI34051 effects. Bars represent from left to right CTR (3/7), PCI34051 (3/7), CTR siRNA (3/7), HDAC8.1+HDAC8.2 (3/7), CTR siRNA (5/7) and HDAC8.1+HDAC8.2 (5/7).

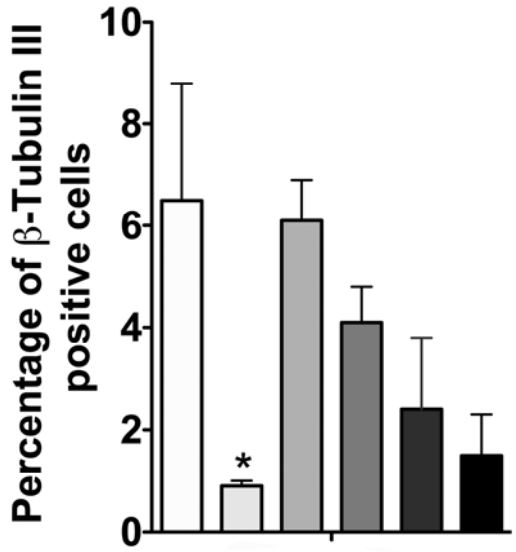

Downloaded from https://academic.oup.com/hmg/advance-article-abstract/doi/10.1093/hmg/ddy329/5098226 by Università degli Studi di Milano user on 28 October 2018

Figure 5. Expression analysis of *hdac8* in zebrafish.

(A-B) RT-PCR performed on different embryonic stages: *hdac8* and □-*actin* expression are shown. *(C-D'') hdac8* Whole mount *in situ* hybridization analyses (WISH) on zebrafish embryos at 24 and 48 hpf developmental stages. *(C)* 24 hpf embryo showing *hdac8* expression in different regions of the CNS (eyes, diencephalon, mesencephalon, hindbrain), in muscles and in the gut. *(C')* Dorsal view (anterior to the left) of the different regions of *hdac8* expression in the CNS. (*C''*) Transverse histological sections (section level is indicated in *C* with black line) of a previously hybridized embryo at 24 hpf. *hdac8* was expressed in the hindbrain. *(D-D') hdac8* WISH at 48 hpf. The transcript persisted in the eyes, diencephalon, mesencephalon, hindbrain and muscles. *hdac8* expression was present also in the fin buds at 48 hpf. *(D'')* Transversal sections of the head at 48 hpf (section level is indicated in *D* with black line). ep: epiboly; e: eye; di: diencephalon; m: midbrain; h: hindbrain, fb: fin bud; mus: muscles; g: gut. Scale bars indicate 100 µm.

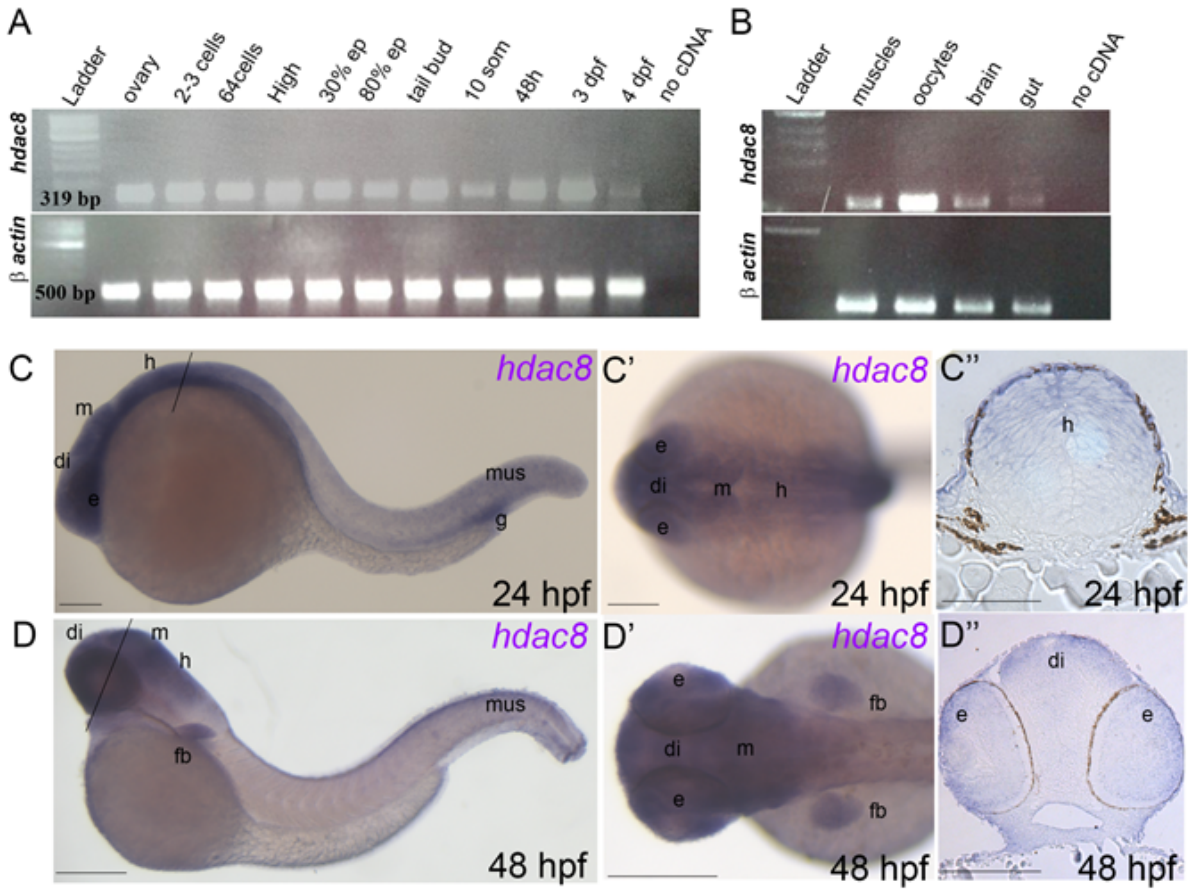

Downloaded from https://academic.oup.com/hmg/advance-article-abstract/doi/10.1093/hmg/ddy329/5098226 by Università degli Studi di Milano user on 28 October 2018

Figure 6. Phenotypical analysis of embryos with *hdac8*-loss-of-function.

(A-D) Phenotypical analysis of embryos at 24 hpf microinjected with *hdac8*-MO *(B, C)* compared to control embryos *(A)*. *(A', C')* higher magnification of the cephalic region of the embryo in *A* and *C*. (*D)* Quantification of embryos microinjected with *hdac8*-MO presenting phenotypes with different degree of severity classified as: class I mild phenotype and class II severe phenotype. *(E-F)* Western blot analyses showed reduced levels of Hdac8 (42 kDa) in the 24 hpf ATG-*hdac8*-MO injected embryos compared to controls at the same developmental stage *(E)* and in splice-*hdac8*-MO injected embryos compared to controls at the same developmental stage *(F)*. Gapdh (36 kDa) housekeeping in *(E)* and Vinculin (120 kDa) in *(F)*. *(G)* RT-PCR performed on control and splice-*hdac8*-MO injected embryos at 24 hpf. RT-PCR primers were designed in exon1 and intron1 respectively. The amplification product was 277 bp and comprehended the intron1 in splice-*hdac8*-MO injected embryos while in ctrl-MO there was no amplification as the intron1 was removed. Scale bars indicate 100 µm.

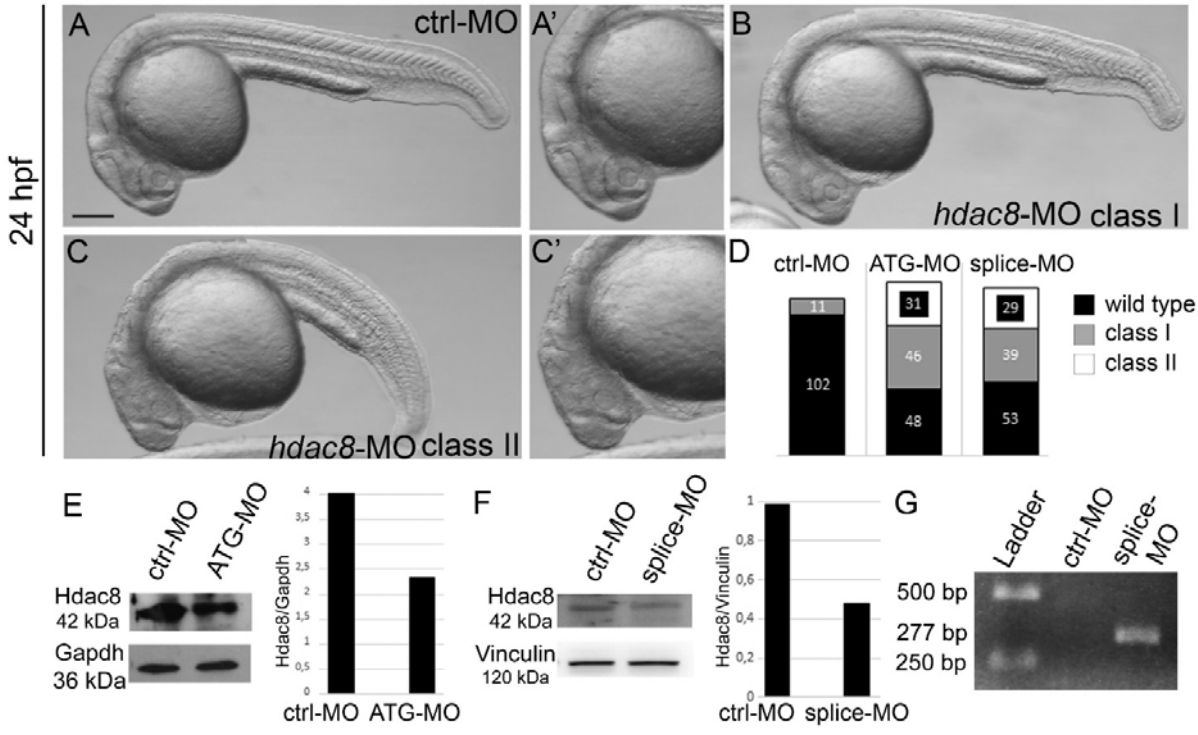

Downloaded from https://academic.oup.com/hmg/advance-article-abstract/doi/10.1093/hmg/ddy329/5098226 by Università degli Studi di Milano user on 28 October 2018

Figure 7. Apoptosis is increased in *hdac8*-MO-injected embryos and rescued by LiCl treatment or *hdac8*-mRNA injection.

(A-C) Analysis of the apoptotic cells by visual TUNEL staining in embryos at 24 hpf microinjected with *hdac8*-MO *(B)* compared to control embryos *(A)*. Dying cells were present in particular at the level of the CNS (arrows in brain and spinal cord) and in optic vescicles as shown by transverse histological sections carried out at the level of the black line (I-II) in A and B *(A^{I},A^{II},B^{I},B^{II})*. *(C)* Reduced apoptosis in *hdac8*-MO injected embryos upon LiCl treatment. *(D)* Reduced apoptosis was also observed in embryos co-injected with splice-*hdac8*-MO and *hdac8*/mRNA. Scale bar indicates 100 μm.

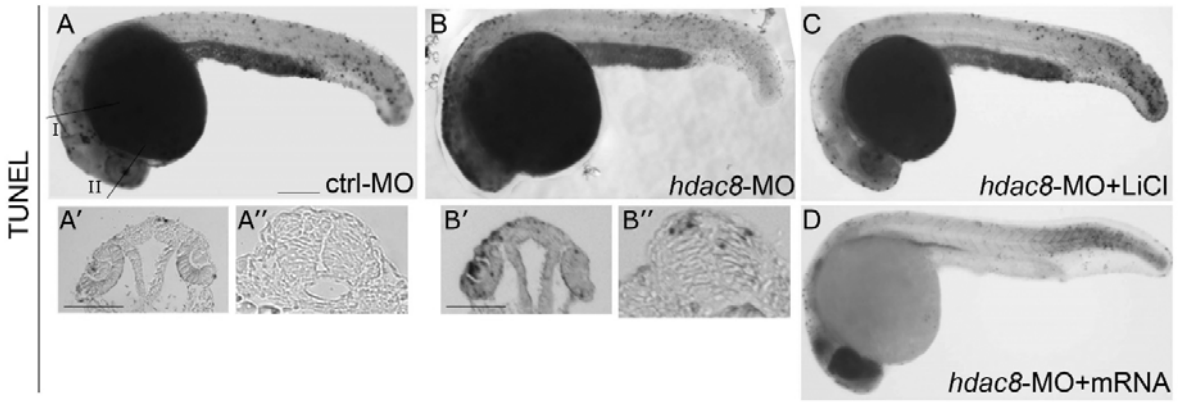

Downloaded from https://academic.oup.com/hmg/advance-article-abstract/doi/10.1093/hmg/ddy329/5098226 by Università degli Studi di Milano user on 28 October 2018

Figure 8. Specificity of the apoptotic phenotype observed following *hdac8* haploinsufficiency

The increased apoptosis was specifically due to the *hdac8* haploinsufficiency as it was obtained by injecting of the two different ATG and splice-*hdac8*-MO. *(A-C)* Specificity of the apoptotic phenotype following *hdac8*-loss-of-function. The increased apoptotic levels were present in both ATG- and splice-*hdac8*-MO-injected embryos *(B-C)* in comparison to controls *(A)*. Fluorescent TUNEL staining in embryos injected with different morpholinos confirmed the specificity of the phenotype. The class II embryos *(B'-C')* presented more apoptotic cells than embryos of class I *(B-C)*. *(D)* Injection of subcritical doses of ATG- and splice-*hdac8*-MO that singularly did not generate apoptosis, demonstrated a synergistic effect on apoptotic levels. CNS: Central Nervous System; SC: Spinal Cord; di: diencephalon; h: hindbrain, n: notocord. Scale bar indicates 100 µm.

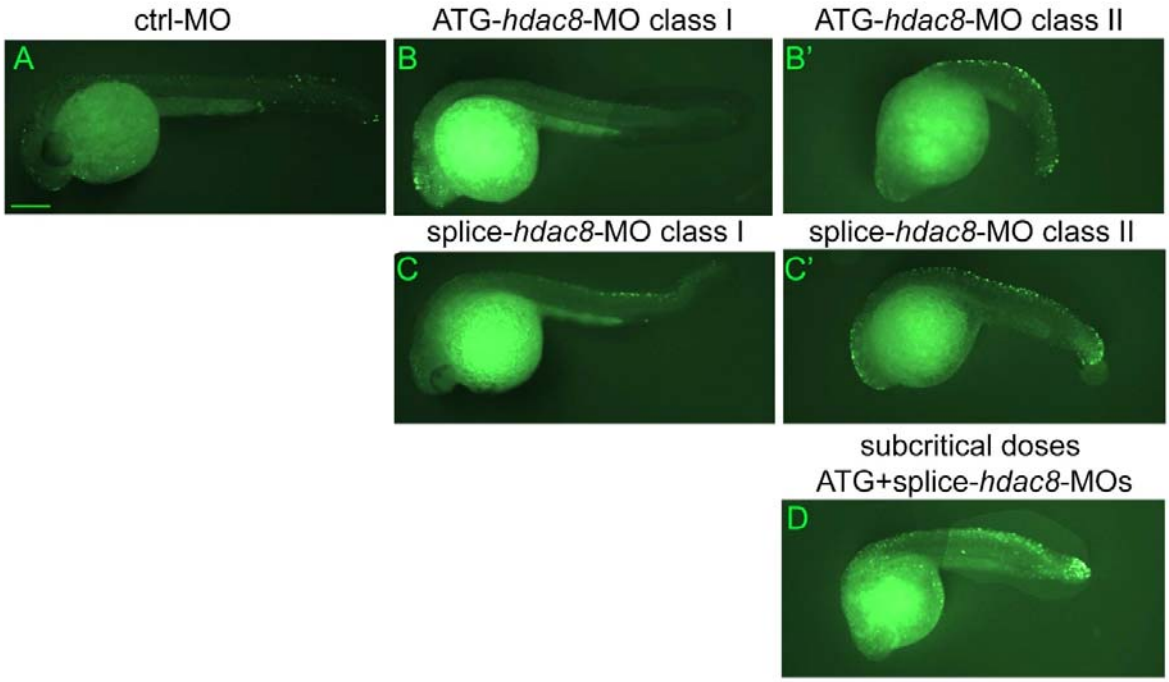

Downloaded from https://academic.oup.com/hmg/advance-article-abstract/doi/10.1093/hmg/ddy329/5098226 by Università degli Studi di Milano user on 28 October 2018

ABBREVIATIONS

Cornelia de Lange Syndrome (CdLS)

Neural stem cells (NSCs)

primitive (p)NSCs

subventricular zone (SVZ)

Whole-mount *in situ* hybridization (WISH)

central nervous system (CNS)

lithium chloride (LiCl)

morpholino (MO)

Cyclin D1 (CCND1)

epidermal growth factor (EGF)

fibroblast growth factor (FGF)

dimethyl sulfoxide (DMSO)

hours post fertilization (hpf)

days post fertilization (dpf)

Reverse transcription-PCR (RT-PCR)

Downloaded from https://academic.oup.com/hmg/advance-article-abstract/doi/10.1093/hmg/ddy329/5098226 by Università degli Studi di Milano user on 28 October 2018